Effect of nanofiber proximity on the mechanical behavior of high volume fraction aligned carbon nanotube arrays

Citation: Cebeci, Hülya, Itai Y. Stein, and Brian L. Wardle. "Effect of Nanofiber Proximity on the Mechanical Behavior of High Volume Fraction Aligned Carbon Nanotube Arrays." Appl. Phys. Lett. 104, no. 2 (January 13, 2014): 023117.

As Published: http://dx.doi.org/10.1063/1.4862273

Publisher: American Institute of Physics

Persistent URL: http://hdl.handle.net/1721.1/86881

Version: Author's final manuscript: final author's manuscript post peer review, without publisher's formatting or copy editing

Effect of Nanofiber Proximity on the Mechanical Behavior of High Volume Fraction Aligned Carbon Nanotube Arrays

Hülya Cebeci,[1,2,a] Itai Y. Stein,[3,a] and Brian L. Wardle[1,b]
[1] *Department of Aeronautics and Astronautics, Massachusetts Institute of Technology, 77 Massachusetts Ave, Cambridge, MA 02139, USA.*
[2] *Department of Aeronautical Engineering, Istanbul Technical University, Maslak 34469, Istanbul, Turkey.*
[3] *Department of Mechanical Engineering, Massachusetts Institute of Technology, 77 Massachusetts Ave, Cambridge, MA 02139, USA.*

The effect of nanofiber proximity on the mechanical behavior of nanofiber arrays with volume fractions (V_f) from 1 to 20% was quantified via nanoindentation of an aligned carbon nanotube (A-CNT) array. The experimental results show that the indentation modulus for A-CNT arrays has a highly non-linear scaling with the CNT V_f, leading to modulus enhancements of up to $\sim 600\times$ at $V_f = 20\%$. Modeling illustrates that the origin of the highly non-linear trend with V_f is due to the minimum inter-CNT spacing, which is shown to be more than an order of magnitude larger than the graphitic spacing.

The demand for miniaturization and increased performance of next-generation devices requires nanostructured materials with controlled properties.[1–5] The highly anisotropic intrinsic thermal, electrical, and mechanical properties of nanowires (NWs), nanofibers (NFs), and nanotubes make them some of the prime candidates.[5] When organized into NF arrays, the fabrication of highly scalable nanostructured architectures becomes possible.[5] However, at NF volume fractions (V_f) exceeding 10 vol. %, where the inter-NF spacing approaches the diameter of the NFs,[6] the usual assumption of negligible NF proximity effects may no longer hold, and a quantification of this effect on the physical properties of the array is necessary. In this letter, the impact of NF proximity effects, a function of the NF V_f,[6] on the mechanical behavior of a controlled morphology aligned NF array is presented for the first time.

To evaluate the effect of NF V_f on the properties of an aligned NF array, an exemplary system of NFs is studied. This system is comprised of aligned multiwalled carbon nanotubes (A-CNTs), which have interesting intrinsic physical properties.[5] Previous studies have managed to use mechanical characterization techniques, such as compression,[7,8] nanoindentation,[8–13] and drop-ball testing,[14–16] to modify traditional continuum mechanics models to enable the quantification of the intrinsic elastic modulus of CNTs in aligned arrays. However, the mechanisms at work in the porous A-CNT arrays, particulary the NF proximity effects, which lead to a measured indentation modulus that is more than six orders of magnitude lower than the theoretical intrinsic modulus of individual CNTs,[8–12] $\simeq 1$ TPa,[17] need further study.[18] In this letter, nanoindentation is used to measure the effective elastic modulus of the A-CNT arrays at CNT V_f ranging from ~ 1 to 20% (average inter-CNT spacing ranging from ~ 80 to 10 nm), and a theoretical model is developed to evaluate the effect of CNT proximity on the mechanical response of the A-CNT arrays.

The A-CNT arrays used in the nanoindentation experiments were grown via a previously described thermal catalytic chemical vapor deposition process using ethylene as the carbon source.[19–22] The CNTs were grown on 1 cm $\times$ 1 cm Si substrates forming CNT arrays that are ~ 1 mm tall, and are composed of multiwalled CNTs that have an average outer diameter of ~ 8 nm ($3-7$ walls with an inner diameter of ~ 5 nm and intrinsic CNT density of ~ 1.7 g/cm^3),[23,24] inter-CNT spacing of ~ 80 nm,[6] and V_f of $\sim 1\%$ CNTs.[23] The A-CNT arrays are then delaminated from the Si substrate using a standard lab razor blade, and mechanically densified (biaxially) to the desired V_f (up to $\sim 20\%$).[6,25] Next, the A-CNT arrays were attached to a steel plate with an adhesive, and inspected under a scanning electron microscope (SEM) for any defects. See Fig. 1 for an SEM micrograph of a densified (~ 20 vol. %) A-CNT array showing some CNT waviness.

Since nanoindentation is sensitive to spatial homogeneities,[26] extra care was taken to ensure the smoothness of the exposed A-CNT surface. To do so, all A-CNT arrays were mounted so that the side previously in contact with the catalyst layer was exposed, thereby avoiding the entangled ~ 1 μm thick growth initiation region,[27] and densified A-CNT arrays ($V_f = 10$ and 20% CNTs) were also machined via 1064 nm and 816 nm wavelength neodymium-doped yttrium aluminum garnet (Nd:YAG) lasers. The laser ablation process consisted of irradiating a 100 μm $\times$ 100 μm region of the arrays with the 1064 nm and 816 nm wavelength lasers at 50 mW for 60 seconds using $\sim 2-2.5\times$ zoom. More details can be found elsewhere.[28] See Fig. 1 for an SEM micrograph of a laser ablated region of an A-CNT array with $V_f = 10\%$ CNTs.

Since tip geometry features on the order of heterogeneity of the A-CNTs (average inter-CNT spacing on the order of $10-80$ nm)[6] can influence the inferred modulus, experiments were carried out using two types of indentors (see Fig. 1 for an illustration of their geometry): a three

[a] H.C. and I.Y.S. contributed equally to this work
[b] Electronic mail: wardle@mit.edu

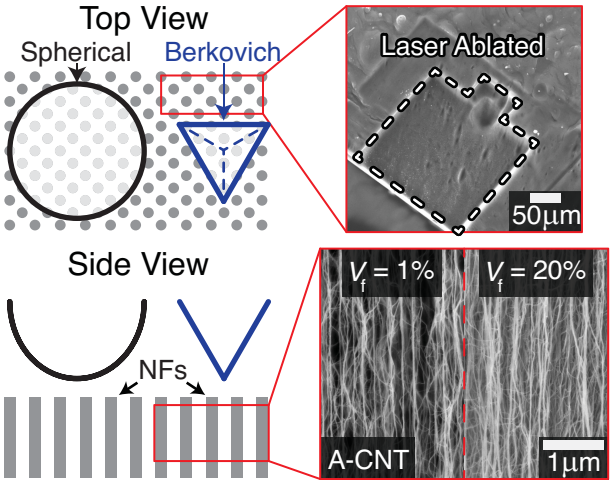

FIG. 1. Indentor and sample geometries, and SEM micrographs of the (laser ablated) top and cross-sectional surfaces of densified A-CNT arrays.

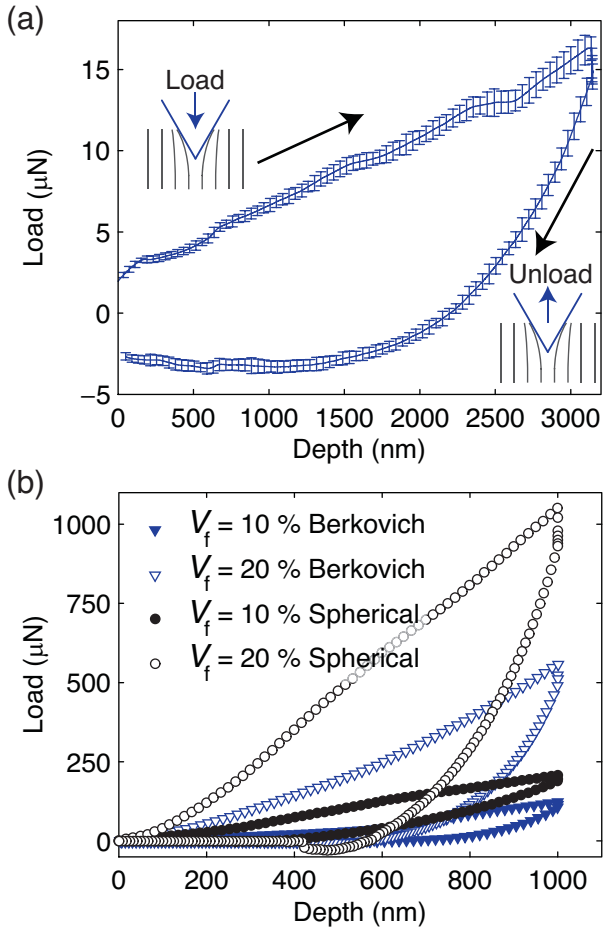

FIG. 2. (a) Average loading curve with standard deviations for 25 indentations of 1 vol. % A-CNT arrays using a Berkovich indentor. (b) Sample loading curves for A-CNT arrays with V_f = 10 and 20% using Berkovich and Spherical indentors.

sided pyramidal (Berkovich) tip with a nominal tip radius of 80 nm; and a conical tip, known as a Spherical tip, that terminates with a 5 μm tip radius and, an apex angle of 60°.[28] The use of these two different indentors allows the effect of indentor geometry to be considered, particularly since the relatively sharp Berkovich tip radius is on the order of the average inter-CNT spacing at $V_f \simeq 1\%$, where the Spherical indentor might give a more accurate representation of the A-CNT forest stiffness. The indentation machine (Turboindenter from Hysitron, Inc.) used for the experiments allowed control over either indentation force or depth, and was capable of a maximum load and displacement of 10 mN and 5 mm, with resolutions of 1 nN (load) and 5 nm (displacement). Calibration was performed for each set of indentations using a standard fused silica specimen interpreted using the method developed by Oliver and Pharr.[28–30] A trapezoidal load profile was used in all indentation tests with a hold time of 5 seconds. To quantify the mechanical behavior of the A-CNT arrays, nanoindentation tests with controlled depths (3 μm for 1 vol. % A-CNT arrays, and 1 μm for 10 and 20 vol. % A-CNT arrays to ensure a linear elastic response) were performed, and the initial slope of the unloading curves was used to evaluate the effective elastic modulus, known as the indentation modulus (E), of the A-CNT arrays using the Oliver and Pharr method.[28–30] See Fig 2 for an averaged loading curve of 25 indentations (smoothed using a 64 point moving average filter) for as-grown 1 vol. % A-CNT arrays (Fig 2a) tested with a Berkovich indentor, and exemplary loading curves for densified 10 and 20 vol. % A-CNT arrays (Fig 2b) tested with both Spherical and Berkovich indentors.

As illustrated by Fig 2a, at an indentation depth of ~ 2.5 μm, a plateau can be seen in the averaged loading curve for the 1 vol. % A-CNT arrays, where the standard deviations illustrate minimal sample variability. Based on a previously reported study on 50 nm outer diameter, $\sim 50-100$ nm tall, $\sim$3 vol. % A-CNT arrays,[31] this distinct drop in slope may correspond to buckling of the CNTs. However, while the previous study estimated the critical buckling at $\sim 2-2.5$ μN independent of the CNT length,[31] Fig. 2a leads to a higher estimated critical buckling load of $\sim 12-14$ μN. This difference in critical buckling load may be attributed to a more imperfect coupling (weaker frictional effects) of the smaller diameter CNTs used here.[18] Also, because no drops in slope can be seen in the loading curves of the densified A-CNT arrays (Fig. 2b) for indentations using both the Spherical and Berkovich tips, we conclude that buckling of CNTs does not occur to a significant degree at 10 vol. % $\lesssim V_f \lesssim$ 20 vol. % at indentation depths of $\lesssim 1$ μm. The lack of buckling in this range of V_f is likely due to the higher CNT proximity, which causes more CNTs to be in contact with the tip and limits the distance CNTs can deflect before interacting with one another, making bending the dominant deformation mechanism.[18] At higher V_f, the CNTs bend and reinforce each other, as in the classic

TABLE I. Indentation moduli and specific stiffness for the Berkovich (E_b) and Spherical (E_s) indentors as a function of the CNT volume fraction (V_f) and average inter-CNT spacing (Γ).[6]

V_f (%)	Γ (nm)	E_b (MPa)	E_s (MPa)	E/ρ[a] (MPa × m^3/kg)
1	78.0	1.7 ± 0.2	8.9 ± 0.7	$0.10 - 0.52$
10	18.5	150 ± 11	71.5 ± 5.4	$0.42 - 0.88$
20	10.3	982 ± 108	816 ± 64	$2.4 - 2.9$

[a] $\rho = V_f \times$ CNT intrinsic density.

beam on an elastic foundation problem.[32]

Using the slopes of the load vs. displacements curves, the indentation moduli, E, were computed via the Oliver and Pharr method,[29,30] and can be found in Table I. As Table I illustrates, the stiffness values evaluated for indentations using the Berkovich tip, defined as E_b, show a very strong dependence on V_f, starting at $\sim 1.7 \pm 0.2$ MPa for the as-grown 1 vol. % A-CNT arrays, and increasing to $\sim 150 \pm 11$ MPa for the densified 10 vol. % A-CNT arrays ($\sim 90\times$ enhancement), and $\sim 982 \pm 108$ MPa for the densified 20 vol. % A-CNT NW arrays ($\sim 600\times$ enhancement). The stiffness values evaluated for the indentations performed using the Spherical tip, defined as E_s, show a similar dependence on V_f, starting at $\sim 8.9 \pm 0.7$ MPa for the as-grown 1 vol. % A-CNT arrays, and increasing to $\sim 71.5 \pm 5.4$ MPa for the densified 10 vol. % A-CNT arrays ($\sim 8\times$ enhancement), and $\sim 816 \pm 64$ MPa for the densified 20 vol. % A-CNT arrays ($\sim 90\times$ enhancement). The E values for the densified 20 vol. % A-CNT arrays exceed those previously reported for other tall (lengths $\simeq 0.1 - 1$ mm to avoid substrate effects) A-CNT systems, which were evaluated at $\sim 10 - 100$ MPa.[8–11] A note should be made about E_b evaluated for $V_f = 1\%$ A-CNTs, where the nominal tip diameter (80 nm) is very close to the average inter-CNT spacing (~ 80 nm),[6] meaning that it is likely an underestimate of the stiffness of the A-CNTs at this V_f, i.e., we interpret the spherical indentor to be more accurate at $V_f = 1\%$. Using the CNT density (ρ) of ~ 1.7 g/cm^3,[24] the specific modulus (E/ρ) of the A-CNT arrays can be evaluated at each V_f (see Table I), and used to compare their performance to other engineering materials. These specific moduli values illustrate that the behavior of the A-CNT arrays at $V_f = 1\%$ is similar to flexible polymer foams, but as the V_f is increased, their behavior becomes more similar to rigid polymer foams ($V_f = 10\%$) and natural materials ($V_f = 20\%$), such as wood.[33] To understand the origin of the highly non-linear dependence of E on V_f, the effect of the significant reduction in inter-CNT spacing is analyzed. To do so, a model that quantifies the collective behavior of the CNTs in aligned arrays as a function of V_f during nanoindentation was developed.

To effectively model the CNT deformation that occurs during nanoindentation, the following simplifying assumptions were made: 1) frictional effects in the system (both between CNTs and between the CNTs and the indentor) are negligible; 2) bending of CNTs is the primary mechanism of deformation; 3) the change in E is directly proportional to the number of CNTs affected by the tip; 4) CNT compression and buckling effects are negligible; 5) the CNT deformation is linear elastic in nature; 6) CNT waviness effects can be ignored from a modeling, but not phenomenological, perspective. These assumptions are based on the following observations: no buckling was observed at indentation depths of $\lesssim 1$ μm (see Fig. 2), which is consistent with minimal frictional effects;[18] indentations signatures could not be found when forests were examined under an SEM post-nanoindentation, indicating the full recovery of the A-CNTs; and a recent study on the stress-strain behavior of low volume fractions ($V_f \sim 1\%$) A-CNT arrays showed that the response of these materials is linear elastic material in the range of deformations studied here.[34] The resulting dependence of the measured modulus on V_f is a function of two parameters: the average inter-CNT spacing, Γ, whose dependence on V_f for A-CNT arrays was previously studied (see Table I for Γ evaluated for A-CNT arrays);[6] and the minimum inter-CNT spacing, defined as Γ_{min}, which is a function of the inter-CNT electrostatic interactions, and does not depend on V_f (the CNTs are not damaged by the densification process). Γ_{min} physically represents the inter-CNT separation at which two A-CNTs can no longer approach one another due to inter-CNT interactions (e.g van der Waals). Γ_{min} is motivated by previous observations that the mechanical densification technique used here cannot yield densified A-CNT arrays with V_f exceeding ~ 40 % ($\Gamma \sim 4.5 - 5.5$ nm).[6] Using these assumptions and parameters, a scaling relationship that could be generalized to other elastic NW and NF systems is developed. The derived scaling relationship in its most simplified form can be found below (see Eq. S1−S9 and Fig. S1 in the Supplementary Information[35] for model development details):

$$E(V_f) \simeq E_{1\%} \left(\frac{\Gamma_{1\%} - \Gamma_{min}}{\Gamma(V_f) - \Gamma_{min}} \right)^2 \quad (1)$$

This scaling behavior is significantly different from the one recently reported for nanoporous zeolitic imidazolate frameworks (ZIFs) tested using a Berkovich tip, which show an empirical $E \propto V_f^2$ scaling relationship (in MPa).[36] See Fig. 3 for a plot of E vs. V_f comparing Eq. 1 (assuming $E_{1\%} \sim 4$ MPa) with the ZIF scaling,[36] and the experimental data from Table I. See Table S1 in the Supplementary Information[35] for the model predicted values for $E(V_f = 10\%)$ and $E(V_f = 20\%)$ at 1 nm $\lesssim \Gamma_{min} \lesssim 7$ nm. As Fig 3 illustrates, both Eq. 1 (at 4 nm $\lesssim \Gamma_{min} \lesssim 6$ nm) and the ZIF scaling equation are in good agreement with the experimental data at $V_f <= 10\%$, but when NF proximity effects become significant ($V_f > 10\%$), the ZIF scaling is no longer representative of the A-CNT array behavior. This is likely due to a difference in pore morphologies, and particle (i.e. nanocrystal) size and aspect ratios between the two systems. Future studies should

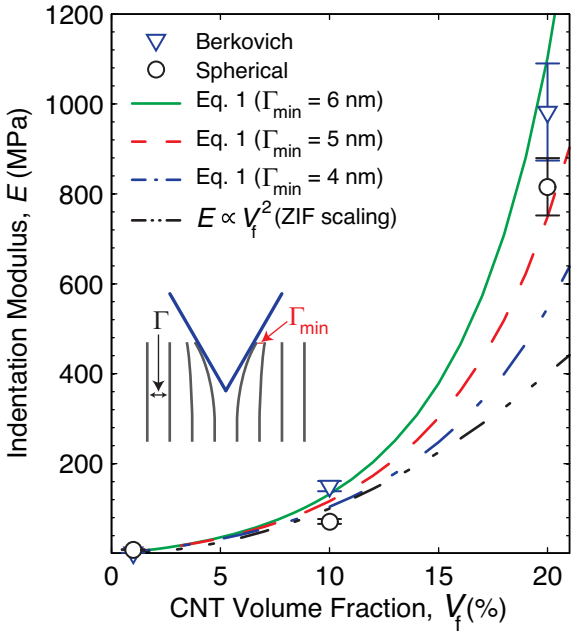

FIG. 3. Comparison of the indentation modulus (see Table I) to the model predictions (Eq. 1) as a function of the minimum spacing, Γ_{min}, and the previously reported scaling relationship of zeolitic imidazolate frameworks, ZIFs ($E \propto V_f^2$).[36]

further explore the origin of Γ_{min} and better approximate its value. Also, although Eq. 1 assumes that the NFs are perfectly collimated, real NFs have some degree of waviness (see Fig. 1). Previous studies have determined that the CNT waviness has a very strong influence on the mechanical behavior of polymer nanocomposites comprised of A-CNT arrays,[37,38] and that the CNT V_f strongly affects the average waviness in the A-CNT arrays.[6,37,38] However, while NF waviness has a strong influence on the mechanical properties of NF arrays, models that enable precise and complete quantification are not currently available,[6] and the incorporation of NF waviness into Eq. 1 was not possible. Future work should include a further study of this effect. Once NF waviness can be properly modeled, the theory developed in this letter will need to be modified to include this additional parameter, and more accurate predictions of the indentation modulus as a function V_f may become possible.

In summary, the effect NF proximity on the mechanical behavior of NF arrays with a NF volume fraction (V_f) up to 20% was quantified both experimentally, via nanoindentation of an A-CNT array, and theoretically. The experimental results show that the indentation modulus for A-CNT arrays scales non-linearly with the CNT V_f, showing enhancements of up to a $\sim 90\times$ for the Spherical tip, and $\sim 600\times$ for the Berkovich tip, at $V_f = 20\%$. The modeling results illustrate that the indentation modulus for A-CNT arrays strongly depends on two parameters: (i) the inter-CNT spacing, a non-linear function of the CNT V_f;[6] (ii) the minimum inter-CNT spacing, a constant that does not depend on CNT V_f, whose value is shown to exceed the graphitic spacing ($\sim$ 0.34 nm) by more than an order of magnitude. Further study on the origin of the minimum inter-CNT spacing is required. The model predictions, while closely resembling the observed behavior of the A-CNT arrays, were still imperfect because a model that allows the precise quantification of the CNT waviness, a factor that could strongly influence the indentation modulus,[37] is not currently available. Future studies should include the modification of the current theory to account for non-negligible CNT waviness and frictional effects. Using these results, aligned NW and NF architectures with controlled properties can be designed for next-generation multifunctional materials and devices.

This work was supported by Boeing, EADS, Embraer, Lockheed Martin, Saab AB, Hexcel, and TohoTenax through MIT's Nano-Engineered Composite aerospace STructures (NECST) Consortium and was supported (in part) by the U.S. Army Research Office under contract W911NF-07-D-0004 and W911NF-13-D-0001. H.C. acknowledges support from the Scientific and Technical Research Council of Turkey (TUBITAK) for a 2214-International Research Fellowship Programme. The authors thank Roberto Guzman de Villoria (MIT), Alan Schwartzmann (MIT) at MIT's NanoMechanical Technology Laboratory, Sunny Wicks (MIT), John Kane (MIT) and the entire necstlab at MIT for technical support and advice. This work made use of the Center for Nanoscale Systems at Harvard University, a member of the National Nanotechnology Infrastructure Network, supported (in part) by the National Science Foundation under NSF award number ECS-0335765, utilized the core facilities at the Institute for Soldier Nanotechnologies at MIT, supported in part by the U.S. Army Research Office under contract W911NF-07-D-0004, and was carried out in part through the use of MIT's Microsystems Technology Laboratories.

[1] W. Lu and C. M. Lieber, Nat. Mater. **6**, 841 (2007).
[2] Q. Cao and J. A. Rogers, Adv. Mater. **21**, 29 (2009).
[3] Z. Fan, J. C. Ho, T. Takahashi, R. Yerushalmi, K. Takei, A. C. Ford, Y.-L. Chueh, and A. Javey, Adv. Mater. **21**, 3730 (2009).
[4] J. A. Rogers, T. Someya, and Y. Huang, Science **327**, 1603 (2010).
[5] M. F. L. De Volder, S. H. Tawfick, R. H. Baughman, and A. J. Hart, Science **339**, 535 (2013).
[6] I. Y. Stein and B. L. Wardle, Phys. Chem. Chem. Phys. **15**, 4033 (2013).
[7] F. Fraternali, T. Blesgen, A. Amendola, and C. Daraio, J. Mech. Phys. Solids **59**, 89 (2011).
[8] C. Cao, A. Reiner, C. Chung, S.-H. Chang, I. Kao, R. V. Kukta, and C. S. Korach, Carbon **49**, 3190 (2011).
[9] C. M. McCarter, R. F. Richards, S. D. Mesarovic, C. D. Richards, D. F. Bahr, D. McClain, and J. Jiao, J. Mater. Sci. **41**, 7872 (2006).
[10] A. A. Zbib, S. D. Mesarovic, E. T. Lilleodden, D. McClain, J. Jiao, and D. F. Bahr, Nanotechnology **19**, 175704 (2008).
[11] A. Qiu, D. Bahr, A. Zbib, A. Bellou, S. Mesarovic, D. McClain, W. Hudson, J. Jiao, D. Kiener, and M. Cordill, Carbon **49**, 1430 (2011).
[12] S. Pathak, Z. G. Cambaz, S. R. Kalidindi, J. G. Swadener, and Y. Gogotsi, Carbon **47**, 1969 (2009).

[13]L. Liu, M. Zhao, Q. Zhou, and X. Chen, Mech. Res. Commun. **35**, 256 (2008).
[14]C. Daraio, V. F. Nesterenko, S. Jin, W. Wang, and A. M. Rao, J. Appl. Phys. **100**, 064309 (2006).
[15]V. R. Coluci, A. F. Fonseca, D. S. Galvão, and C. Daraio, Phys. Rev. Lett. **100**, 086807 (2008).
[16]A. Misra, J. R. Raney, A. E. Craig, and C. Daraio, Nanotechnology **22**, 425705 (2011).
[17]J. P. Lu, Phys. Rev. Lett. **79**, 1297 (1997).
[18]L. F. Wang, C. Ortiz, and M. C. Boyce, J. Eng. Mater. Technol. **133**, 011014 (2011).
[19]E. J. Garcia, B. L. Wardle, A. J. Hart, and N. Yamamoto, Compos. Sci. Technol. **68**, 2034 (2008).
[20]B. L. Wardle, D. S. Saito, E. J. García, A. J. Hart, R. Guzmán de Villoria, and E. A. Verploegen, Adv. Mater. **20**, 2707 (2008).
[21]S. Vaddiraju, H. Cebeci, K. K. Gleason, and B. L. Wardle, ACS Appl. Mater. Interfaces **1**, 2565 (2009).
[22]A. M. Marconnet, N. Yamamoto, M. A. Panzer, B. L. Wardle, and K. E. Goodson, ACS Nano **5**, 4818 (2011).
[23]A. J. Hart and A. H. Slocum, J. Phys. Chem. B **110**, 8250 (2006).
[24]I. Y. Stein, *Synthesis and Characterization of Next-Generation Multifunctional Material Architectures: Aligned Carbon Nanotube Carbon Matrix Nanocomposites*, Master's thesis, Massachusetts Institute of Technology (2013).
[25]L. Liu, W. Ma, and Z. Zhang, Small **7**, 1504 (2011).
[26]V. P. Veedu, A. Cao, X. Li, K. Ma, C. Soldano, S. Kar, P. M. Ajayan, and M. N. Ghasemi-Nejhad, Nat. Mater. **5**, 457 (2006).
[27]M. Bedewy, E. R. Meshot, H. Guo, E. A. Verploegen, W. Lu, and A. J. Hart, J. Phys. Chem. C **113**, 20576 (2009).
[28]H. Cebeci, *Multifunctional Properties of Controlled Morphology Aligned Carbon Nanotube Polymer Nanocomposites and Their Applications*, Ph.D. thesis, Istanbul Technical University (2011).
[29]W. Oliver and G. Pharr, J. Mater. Res. **7**, 1564 (1992).
[30]W. Oliver and G. Pharr, J. Mater. Res. **19**, 3 (2004).
[31]J. F. Waters, P. R. Guduru, M. Jouzi, J. M. Xu, T. Hanlon, and S. Suresh, Appl. Phys. Lett. **87**, 103109 (2005).
[32]E. Winkler, *Die Lehre von der Elastizität und Festigkeit*, 1st ed. (Dominicius, 1867).
[33]M. Ashby, H. Shercliff, and D. Cebon, *Materials: Engineering, Science, Processing and Design* (Elsevier Science, 2007).
[34]M. R. Maschmann, G. J. Ehlert, S. Tawfick, A. J. Hart, and J. W. Baur, Carbon **66**, 377 (2014).
[35]See supplementary material at http://dx.doi.org/10.1063/1.4862273 for additional model derivation information (Eq. S1−S9, Fig. S1), and a Table of model predicted values (Table S1).
[36]J. C. Tan, T. D. Bennett, and A. K. Cheetham, Proc. Natl. Acad. Sci. U. S. A. **107**, 9938 (2010).
[37]H. Cebeci, R. Guzmán de Villoria, A. J. Hart, and B. L. Wardle, Compos. Sci. Technol. **69**, 2649 (2009).
[38]D. Handlin, I. Y. Stein, R. Guzman de Villoria, H. Cebeci, E. M. Parsons, S. Socrate, S. Scotti, and B. L. Wardle, J. Appl. Phys. **114**, 224310 (2013).

Supplementary Information: Effect of Nanofiber Proximity on the Mechanical Behavior of High Volume Fraction Aligned Carbon Nanotube Arrays

Hülya Cebeci,[1,2,a)] Itai Y. Stein,[3,a)] and Brian L. Wardle[1,b)]

[1)] *Department of Aeronautics and Astronautics, Massachusetts Institute of Technology, 77 Massachusetts Ave, Cambridge, MA 02139, USA.*

[2)] *Department of Aeronautical Engineering, Istanbul Technical University, Maslak 34469, Istanbul, Turkey.*

[3)] *Department of Mechanical Engineering, Massachusetts Institute of Technology, 77 Massachusetts Ave, Cambridge, MA 02139, USA.*

[a)] H.C. and I.Y.S. contributed equally to this work

[b)] Electronic mail: wardle@mit.edu

I. MODEL DEVELOPMENT

To predicted the indentation modulus of densified CNT arrays, the 1D repeat units for both the pre-indentation, δ_i, and post-indentation, δ_f states must first be defined using the outer diameter of the CNTs, D_o, and the average pre-indentation, Γ, and post-indentation, $\Gamma_{\min}$, inter-CNT spacing:

$$\Lambda = D_o + \Gamma \tag{S1a}$$

$$\lambda = D_o + \Gamma_{\min} \tag{S1b}$$

Where Γ is calculated using the previously reported continuous nanowire coordination model (see Table 1 in the main text for the computed Γ), and $\Gamma_{\min}$ is defined as the spacing at which electrostatic (e.g. van der Waals) interactions cause CNT bending over further densification.

Next, the width of the indentor that penetrates the surface of the CNT array, W, (see Fig. S1 for illustration) is used along with Λ to determine the average number of CNTs directly affected by the tip during indentation, n:

$$n = \frac{W_i}{\Lambda} \tag{S2}$$

n is then used to determine the final 1D width of the fully densified CNTs that were directly affected by the indentation, w (see Fig. S1 for illustration):

$$w = n\lambda = \left(\frac{W}{\Lambda}\right)\lambda \tag{S3}$$

The total effective line length of CNTs that are affected by the indentation of the tip, both directly and indirectly, is defined as L_e (see Fig. S1 for illustration) and takes the following infinite sum form:

$$L = w + W = \left(\frac{W}{\Lambda}\right)\lambda + \left(\frac{W}{\Lambda}\right)\lambda\left(\frac{\lambda}{\Lambda}\right) + \left(\frac{W}{\Lambda}\right)\lambda\left(\frac{\lambda}{\Lambda}\right)^2 + \ldots \tag{S4}$$
$$\hookrightarrow \left(\frac{W}{\Lambda}\right)\lambda\sum_{j=0}^{\infty}\left(\frac{\lambda}{\Lambda}\right)^j$$

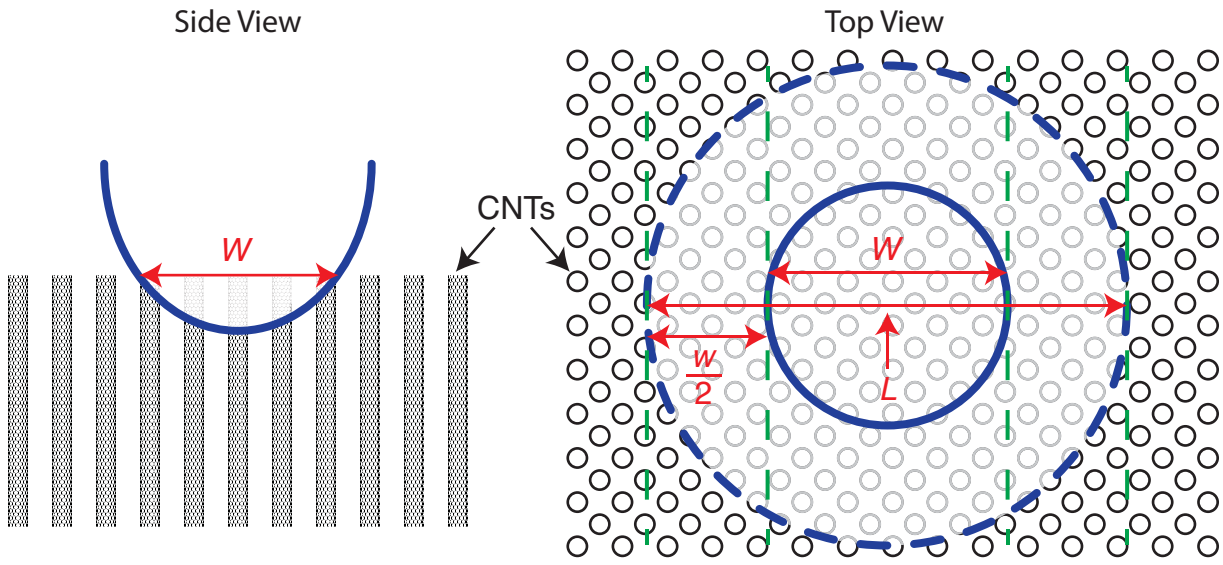

FIG. S1. Illustration of the geometries used to define the 1D pre, W, and post-indentation, w (Eq. S3), CNT widths, and the effective line length of affected CNTs, L (Eq. S5 and Eq. S6).

Eq. S5 converges to the following closed form:

$$L = \left(\frac{W}{\Lambda}\right)\lambda\left(\frac{\Lambda}{\Lambda-\lambda}\right) = W\lambda\left(\frac{1}{\Lambda-\lambda}\right) \tag{S5}$$

Using a factor that depends on the tip geometry, defined as Π, the effective indentation area of the tip, A, can now be evaluated:

$$A = \Pi L^2 \tag{S6}$$

Using Eq. S1, Eq. S6, and Eq. S7, the total number of CNTs affected by the indentation, defined as n^{tot}, can be evaluated:

$$n^{tot} = \frac{A}{\lambda^2} = \Pi W^2\left(\frac{1}{\Lambda-\lambda}\right)^2 \tag{S7}$$

To relate the change in CNT volume fraction, V_{f}, to the measured change in indentation modulus, E, of the system, a scaling factor, Ω, needs to be defined. Ω is then related to the elastic moduli of forests at different two different volume fractions, defined as $\Omega_{1\to2}$, and takes the following form:

$$\Omega_{1\to2} \simeq \frac{n_2^{tot}}{n_1^{tot}} \simeq \frac{\Pi W^2 \left(\frac{1}{\Lambda_1-\lambda}\right)^2}{\Pi W^2 \left(\frac{1}{\Lambda_2-\lambda}\right)^2} \simeq \left(\frac{\Lambda_1-\lambda}{\Lambda_2-\lambda}\right)^2 \tag{S8}$$

Applying $\Omega_{1\to2}$ to predict the the change in indentation modulus for $V_{\mathrm{f},2}$ relative to $V_{\mathrm{f},1}$ yields:

$$E(V_{\mathrm{f},2}) \propto E(V_{\mathrm{f},1})\Omega_{1\to2} \propto E(V_{\mathrm{f},1}) \left(\frac{\Lambda(V_{\mathrm{f},1})-\lambda}{\Lambda(V_{\mathrm{f},2})-\lambda}\right)^2 \tag{S9}$$

Eq. S9 can be re-written as a function of only the average pre and post-indentation inter-CNT spacings, and can be found in the main text (Eq. 1).

TABLE S1. Predicted indentation modulus, E, values for CNT forests with volume fractions, V_{f}, of 10 and 20 vol. % CNTs as a function of the minimum spacing, Γ_{min}, using Eq. 1 of the main text evaluated with $E(V_{\mathrm{f}} = 1\%) \sim 4$ MPa.

Γ_{min} (nm)	$E(V_{\mathrm{f}} = 10\%)$ (MPa)	$E(V_{\mathrm{f}} = 20\%)$ (MPa)
1	77.2	272.1
2	84.6	332.4
3	93.4	418.0
4	103.8	545.5
5	116.5	748.4
6	132.2	1102.4
7	151.9	1810.8